Comparisons between different approximations to energy dissipation rate in a self-preserving far wake

T. Zhou,[1,*] Z. Hao,[2] L. P. Chua,[1] and Y. Zhou[3]
[1]*School of Mechanical and Aerospace Engineering, Nanyang Technological University, Singapore 639798*
[2]*Maritime Research Center, School of Civil and Environmental Engineering, Nanyang Technological University, Singapore 639798*
[3]*Department of Mechanical Engineering, The Hong Kong Polytechnic University, Hung Hom, Kowloon, Hong Kong, China*
(Received 14 June 2006; revised manuscript received 12 September 2006; published 29 November 2006)

By using a four-hot-wire probe and an eight-hot-wire probe, different approximations to energy dissipation rate have been made in the far field of a cylinder wake. The appropriateness of the various approximations is evaluated by examining their mean values, spectra, conditional analysis, and scaling range exponents. It is found that there are significant differences between the instantaneous values of ϵ_{iso}, the isotropic dissipation rate, and other approximations. The present measurements also allow the examination of the spatial correlation between the energy dissipation rate and the enstrophy Ω. While the correlation between ϵ_{iso} and Ω is low, there is a strong correlation between the other approximations to energy dissipation rate ϵ and the enstrophy Ω. The scaling range exponents show that the substitutes to the energy dissipation rate and enstrophy based on isotropy are more intermittent than their corresponding true values. The present results suggest that using ϵ_{iso} as a substitute of ϵ should be re-examined, especially for the instantaneous values.

DOI: 10.1103/PhysRevE.74.056308 PACS number(s): 47.27.Ak

I. INTRODUCTION

The instantaneous values of the turbulent energy dissipation rate $\epsilon(\equiv 2\nu s_{i,j}s_{i,j})$ and the enstrophy $\Omega(\equiv\omega_i\omega_i)$ are two important characteristics of the small-scale turbulence, where $s_{ij}\equiv(u_{i,j}+u_{j,i})/2$ is the turbulent rate of strain; $u_{i,j}$ represents the velocity derivative $\partial u_i/\partial x_j$; $\omega_i=\epsilon_{ijk}u_{k,j}$ is the vorticity component; ϵ_{ijk} is the alternating tensor; and ν is the kinematic viscosity of the fluid. For example, the second-order behavior of the energy dissipation is crucial to understand the characteristics of intermittency [1]. The measurements of ϵ are useful for examining the intermittency models (e.g., [2,3]). However, the measurement of the energy dissipation rate ϵ is fraught of difficulties, since nine velocity derivatives need to be resolved simultaneously. A possible method to measure these velocity derivatives is by using multi-hot-wires. As the number of wires increases, problems related to the spatial resolution of the probe, flow blockage, noise contamination, and possibly aerodynamic interference of the wires become important. Therefore, there are only a few measurements of ϵ reported previously in various turbulent flows (e.g., [4–7]). Most of the ε data used in the literature for examining the small-scale turbulence are obtained by the so-called pseudo-dissipation rate, i.e.,

$$\epsilon_{iso}=15\nu u_{1,1}^2, \tag{1}$$

which is the one-dimensional surrogate of energy dissipation rate ϵ in isotropic turbulence based on Taylor's hypothesis. The limitations of Taylor's hypothesis are relatively well known, especially in flows with high turbulence intensity [8]. It needs to be noted that some important ideas on the small-scale structure of turbulence, such as the multifractal distribution of dissipation in space [9] and the bimodality of conditional probability density functions for a small-scale range [10] of the Kolmogorov variable in the refined similarity hypothesis (RSH) [11], have been reformulated explicitly for ϵ_{iso}. This reformulation has been verified for several cases and therefore can be considered as fundamental at high Reynolds numbers [10]. However, in many aspects, the true values of ϵ may give important different results as compared with those when ϵ_{iso} is used, especially at low and moderate Reynolds numbers [12]. This possibility was pointed out by Hosokawa [13] and Thoroddsen [14] and discussed later in detail by Hosokawa *et al.* [15] and Wang *et al.* [12], using direct numerical simulations (DNS) of fully developed decaying isotropic turbulence at moderate Reynolds numbers. Direct numerical simulations are prior to the experiments since the velocity derivatives can be determined reliably and simultaneously, albeit in relatively simple flows.

The spatial relationship between the fields of ϵ and Ω has been reviewed by Sreenivasan and Antonia [16]. There is general agreement that the highest vorticity appears to reside in tubes, while the moderate vorticity resides in sheets surrounding the tubes. This suggests a relatively high correlation between ϵ and Ω. For homogeneous turbulence, since the mean values of ϵ and Ω are related, i.e., $\langle\epsilon\rangle=\nu\langle\Omega\rangle$, it is natural to expect a close relationship between the instantaneous values of ϵ and Ω. This relation, however, does not mean that their local scaling and intermittence are identical. If they do, however, the scaling exponents for small-scale turbulence should be unique [17]. The existing experimental results surveyed by Sreenivasan and Antonia [16] suggest that the scaling exponents for energy dissipation rate and enstrophy may indeed not be the same, even though the experimental results may be affected in unknown ways by artifacts such as Taylor's hypothesis and the use of one-dimensional surrogates of dissipation and vorticity. By using full measurements for ϵ and Ω obtained in grid turbulence, Antonia *et al.* [6] found that Ω is more intermittent than ϵ. This is consistent with the direct numerical simulations of

*Electronic address: mtmzhou@ntu.edu.sg

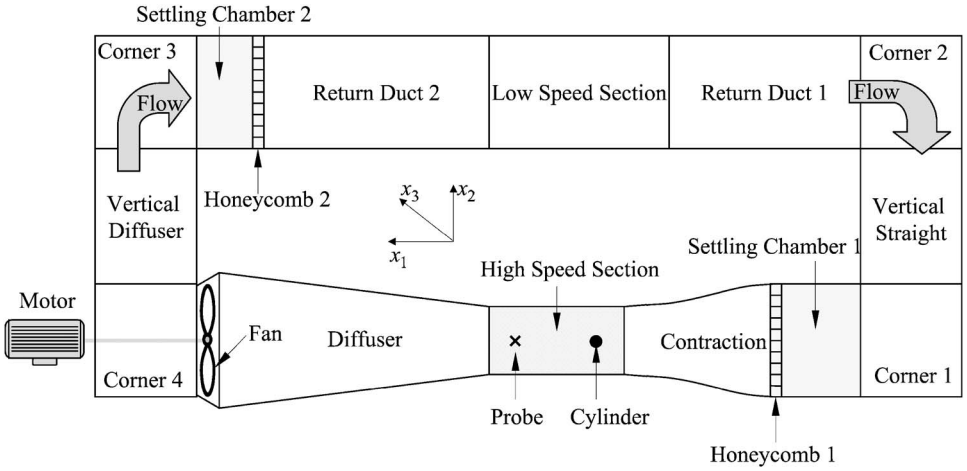

FIG. 1. Schematic diagram of the wind tunnel and the coordinate system.

Chen *et al.* [17], where the inertial range scalings of the locally averaged ϵ and Ω are studied at a Taylor microscale Reynolds number of 216.

The main objective of the present paper is to examine the differences between various substitutes of ϵ using data obtained in the far region of a turbulent wake from a four-hot-wire probe and an eight-hot-wire probe. Differences among various approximations to ϵ will be examined in terms of their mean values, spectra, correlations with the enstrophy fields, and inertial range scaling. After a brief introduction in Sec. I, the experimental setup is given in Sec. II. The mean values of ϵ obtained using different approximations are compared in Sec. III. The differences of various approximations to ϵ are compared in Sec. IV in terms of the correlations with enstrophy. The inertial range scaling of the energy dissipation rate and enstrophy is examined in Sec. V. Conclusions are drawn in Sec. VI.

II. EXPERIMENTAL DETAILS

The experiments were conducted in a closed-loop wind tunnel (Fig. 1). The wind tunnel has two test sections, namely, the high-speed and the low-speed sections. The present measurements are conducted in the high-speed test section with dimensions of 1.2 m (width) $\times$0.8 m (height) and 2 m long. The free stream across the tunnel is uniform to within 0.3%. The free stream turbulence intensity is less than 0.5%. The free-stream velocity U_1 is about 5 m/s, corresponding to a Taylor microscale Reynolds number R_λ ($\equiv u_1'\lambda/\nu$, where $\lambda = u_1'/u_{1,1}'$ is Taylor microscale and the superscript prime denotes the rms value) of about 45 (or $\mathrm{Re}_d \equiv U_1 d/\nu = 2060$, $d = 6.35$ mm is the diameter of the stainless-steel circular cylinder). The measurement location is at $x_1/d = 240$. At this location, the turbulence intensity u_i'/U_1 ($i = 1$, 2, or 3) is about 2%, favoring the use of Taylor's hypothesis. The Kolmogorov length scale η is about 0.5 mm over the vertical range of $x_2/L = \pm 1$, where L is the wake half-width. This value of η is large enough to ensure adequate spatial resolution of the probes for the measurements of the velocity derivatives. With the increase of Reynolds number, the Kolmogorov length scale η will decrease and the spatial resolution of the probes will deteriorate. Therefore, the present experiments were conducted at a relatively low Reynolds number.

A probe consisting of four hot wires [Fig. 2(a)] was used to measure approximately the energy rate. Wires a and b in [Fig. 2(a)] together form the X-wire; wires c and d are the two parallel wires which straddle the X-wire. The solid thin line at the center of wires a, b, c, or d represents the active part (i.e., the sensor) of the four hot wires. β is the angle between flow direction and wire a. The four hot wires also allow the calculation of the spanwise component ω_3 of the vorticity vector using the measured velocity signals u_1 and u_2. The included angle of the X-wire is about 100°. The separation Δx_2 between the two parallel hot wires c and d is about 1.5 mm. This separation corresponds to 3η in the central part of the wake. This separation is adequate for velocity-derivative measurements using hot wires [18]. Us-

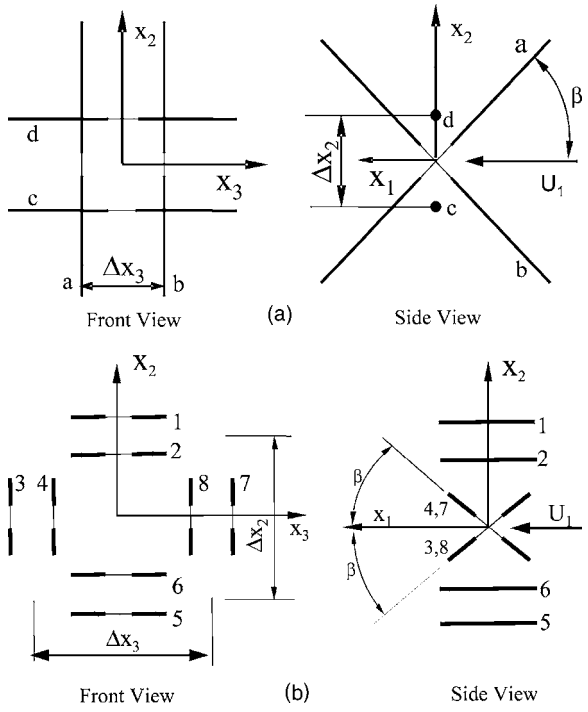

FIG. 2. Sketches of the (a) four-hot-wire and (b) eight-hot-wire probes.

ing the present probe, three of the nine velocity derivatives that make up ϵ are measured simultaneously. These derivatives are $u_{1,1}$, $u_{1,2}$, and $u_{2,1}$. Assuming local isotropy and homogeneity, simultaneous approximations to ϵ can be made based on continuity [19], viz.

$$\epsilon_{ap} \approx \nu(6u_{1,1}^2 + 3u_{1,2}^2 + 2u_{2,1}^2 + 2u_{1,2}u_{2,1}), \tag{2}$$

where the subscript *ap* represents "approximation." Since more derivative correlations are included in Eq. (2) than the one usually used by experimentalists after assuming local isotropy [Eq. (1)], it is expected that Eq. (2) should provide more reasonable approximations to ϵ than when ϵ_{iso} [Eq. (1)] is used. With the present four hot-wire probe, the spanwise vorticity component ω_3 can be obtained viz.

$$\omega_3 = u_{2,1} - u_{1,2} \approx \frac{\Delta u_2}{\Delta x_1} - \frac{\Delta u_1}{\Delta x_2}, \tag{3}$$

where Δu_1 is the velocity difference between the longitudinal velocity fluctuations from the two parallel wires c and d, which are separated in the x_2 direction [Fig. 2(a)]. Δu_2 represents the difference between values of u_2 at the same point in space but separated by one sampling time interval $\Delta t(\equiv 1/f_s)$. In Eqs. (1)–(3), Taylor's hypothesis is used to estimate the velocity derivatives in the streamwise direction, i.e., $\partial u_2/\partial x_1 = -U_1^{-1}\Delta u_2/\Delta t$.

The probe used to measure the full energy dissipation rate consists of four X-wires [Fig. 2(b)]. Two are in the x_1-x_2 plane and separated in the x_3 direction; the other two are in the x_1-x_3 plane and are separated in the x_2 direction. It is assumed that each X-wire measures two velocity components at the center of the probe. The separation between two inclined wires in each pair of X-wire is about 1 mm. The separation between the centers of the two X-wires aligned either in the x_1-x_2 plane and separated in the x_3 direction or the x_1-x_3 plane and separated in the x_2 direction is about 2.7 mm, i.e., around 5η, which satisfies the criteria of hot-wire separation $(3 \sim 5\eta)$ for velocity derivative measurements proposed by Antonia *et al.* [18].

The effective angle for each X-wire is about 40°. The full expression for the mean energy dissipation rate $\langle\epsilon\rangle \equiv 2\nu\langle s_{i,j}s_{i,j}\rangle$ can be written as

$$\begin{aligned}\langle\epsilon_f\rangle \equiv \nu\{&2\langle u_{1,1}^2\rangle + 2\langle u_{2,2}^2\rangle + 2\langle u_{3,3}^2\rangle + \langle u_{1,2}^2\rangle + \langle u_{2,1}^2\rangle + \langle u_{1,3}^2\rangle \\ &+ \langle u_{3,1}^2\rangle + \langle u_{2,3}^2\rangle + \langle u_{3,2}^2\rangle + 2\langle u_{1,2}u_{2,1}\rangle + 2\langle u_{1,3}u_{3,1}\rangle \\ &+ 2\langle u_{2,3}u_{3,2}\rangle\},\end{aligned} \tag{4}$$

where the subscript f represents the full energy dissipation rate. Seven of the above nine velocity derivatives can be obtained with the eight-wire probe. By assuming incompressibility, the quantities $u_{2,2}^2$ and $u_{3,3}^2$ can be estimated by the following equation:

$$u_{1,1} + u_{2,2} + u_{3,3} = 0 \tag{5}$$

or

$$2\langle u_{2,2}^2\rangle + 2\langle u_{3,3}^2\rangle = 2\langle u_{1,1}^2\rangle - 4\langle u_{2,2}u_{3,3}\rangle. \tag{6}$$

By assuming homogeneity, the last term on the right of Eq. (6) can be replaced by $-4\langle u_{2,3}u_{3,2}\rangle$, since

$$\langle u_{2,2}u_{3,3}\rangle = \langle u_{2,3}u_{3,2}\rangle. \tag{7}$$

Substitution of Eqs. (6) and (7) into Eq. (4) yields

$$\begin{aligned}\langle\epsilon_f\rangle \equiv \nu\{&4\langle u_{1,1}^2\rangle + \langle u_{1,2}^2\rangle + \langle u_{2,1}^2\rangle + \langle u_{1,3}^2\rangle + \langle u_{3,1}^2\rangle + \langle u_{2,3}^2\rangle \\ &+ \langle u_{3,2}^2\rangle + 2\langle u_{1,2}u_{2,1}\rangle + 2\langle u_{1,3}u_{3,1}\rangle - 2\langle u_{2,3}u_{3,2}\rangle\}.\end{aligned} \tag{8}$$

By using the measured velocity signals from the eight-wire probe, the three vorticity components can be calculated using the following finite difference method $\partial u_i/\partial x_j = \Delta u_i/\Delta x_j$, i.e.,

$$\omega_1 = u_{3,2} - u_{2,3} \approx \frac{\Delta u_3}{\Delta x_2} - \frac{\Delta u_2}{\Delta x_3}, \tag{9}$$

$$\omega_2 = u_{1,3} - u_{3,1} \approx \frac{\Delta u_1}{\Delta x_3} - \frac{\Delta u_3}{\Delta x_1}, \tag{10}$$

and

$$\omega_3 = u_{2,1} - u_{1,2} \approx \frac{\Delta u_2}{\Delta x_1} - \frac{\Delta u_1}{\Delta x_2}. \tag{11}$$

The streamwise derivatives are calculated using Taylor's hypothesis, i.e., $\partial u_i/\partial x_1 = -U^{-1}\Delta u_i/2\Delta t$ $(i=2,3)$, where U is the local mean velocity and $\Delta t(\equiv 1/f_s)$ is one sampling time interval. This method would have the advantage of keeping $\Delta x_1 \approx \Delta x_2 \approx \Delta x_3$.

Both the four- and eight-wire probes comprised 2.5-μm-diameter Wollaston Pt-10%Rh wires, each etched to an active length of about 0.5 mm. The length-to-diameter ratio of the wires was about 200. The hot wires were operated with in-house constant temperature circuits at an overheat ratio of 1.5. The probes were calibrated at the centerline of the wind tunnel against a Pitot-static tube. The yaw calibration was performed over ±20°. The output signals from the anemometers were passed through buck and gain circuits and low-pass filtered at a cutoff frequency $f_c \equiv 1600$ Hz, which is close to f_K, where $f_K \equiv U/2\pi\eta$ is the Kolmogorov frequency. The filtered signals are sampled for 60 s at a frequency of 3200 Hz into a PC using a 16-bit A/D converter.

III. MEAN ENERGY DISSIPATION RATES

The mean energy dissipation rates $\langle\epsilon\rangle$ obtained using Eqs. (1), (2), and (8) across the wake for different x_2/L are compared in Fig. 3, where L is the wake half-width. In this figure, the energy dissipation rate is normalized by L and the maximum velocity deficit U_0. Since more derivative correlations are included in Eqs. (2) and (8), it is expected that they should provide more reasonable approximations to ϵ than when ϵ_{iso} [Eq. (1)] is used. To account for the effect of the imperfect spatial resolution, all velocity derivatives involved in these relations have been corrected using spectral method. Details of the correction methods for the four-hot-wire and eight-hot-wire probes can be found in Antonia *et al.* [20] and Zhu and Antonia [21], respectively. Figure 3 shows that the magnitude of $\langle\epsilon_f\rangle$ is about 10% larger than that of $\langle\epsilon_{iso}\rangle$ across the wake, which should be in the range of experimental uncertainty, indicating that the one-dimensional surrogate

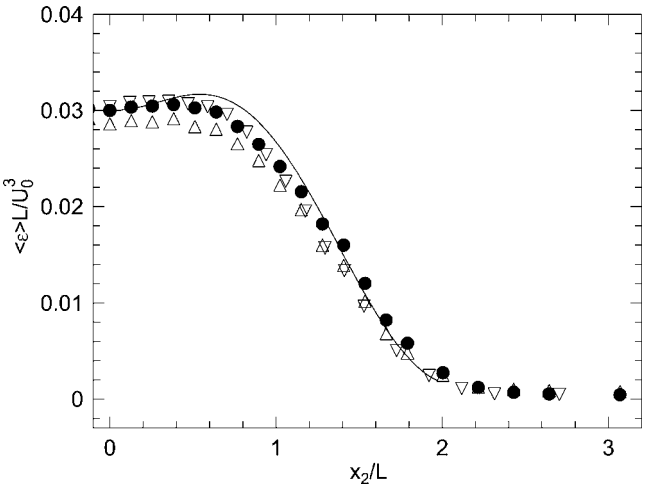

FIG. 3. Comparison of the mean turbulent energy dissipation rate $\langle\epsilon\rangle$ obtained using different approximations: ∇, $\langle\epsilon_f\rangle$ [Eq. (8)]; ●, $\langle\epsilon_{ap}\rangle$ [Eq. (2)]; Δ, $\langle\epsilon_{iso}\rangle$ [Eq. (1)]; and —, Browne *et al.*[22].

can represent the full mean energy dissipation rate properly. The present results of $\langle\epsilon_f\rangle$ also agree favorably with that of $\langle\epsilon_{ap}\rangle$ obtained using the four-wire probe [Eq. (2)]. These latter values of $\langle\epsilon\rangle$ agree well with that reported by Browne *et al.* [22]. The satisfactory agreement shown in Fig. 3 indicates that there is no apparent difference of the measured $\langle\epsilon\rangle$ when different approximations of ϵ were used.

The spectra corresponding to the energy dissipation rates obtained on the wake centerline using different methods are compared in Fig. 4, where a superscript asterisk denotes normalization by Kolmogorov length scale η and/or velocity scale $u_K(\equiv\nu/\eta)$. These spectra are obtained by summing all the spectra of the velocity derivatives involved in Eqs. (1), (2), and (8), respectively. Since the velocity derivative spectra are normalized by the Kolmogorov scales, the areas under the various distributions of the energy dissipation rate should be equal to 1. The distribution of $\phi_{\epsilon_{ap}}(k_1)$ agrees well with that of $\phi_{\epsilon_f}(k_1)$, indicating that Eq. (2) could provide a good approximation to the full energy dissipation rate. In contrast,

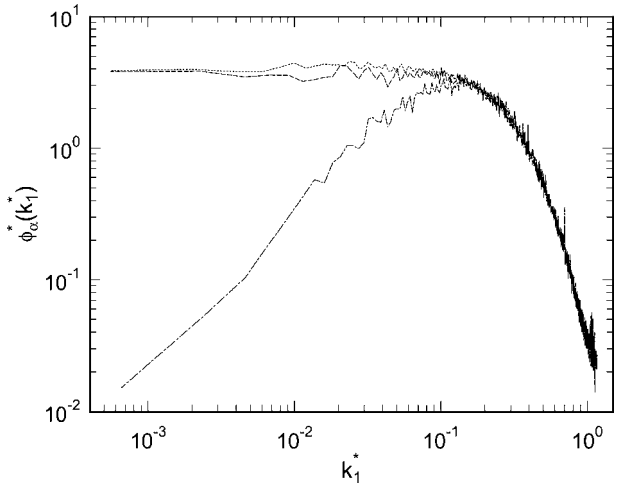

FIG. 4. Spectra of energy dissipation rate obtained using various methods: – – –, $\Phi^*_{\epsilon_{ap}}(k_1^*)$; - - -, $\Phi^*_{\epsilon_f}(k_1^*)$; and — · —, $\Phi^*_{\epsilon_{iso}}(k_1^*)$.

$\phi_{\epsilon_{iso}}(k_1)$ departs significantly from both $\phi_{\epsilon_f}(k_1)$ and $\phi_{\epsilon_{ap}}(k_1)$, except for $k_1^*>0.15$. Since $\phi_{\epsilon_{iso}}(k_1)=15\phi_{\partial u_1/\partial x_1}(k_1)$, the spectrum of ϵ_{iso} is actually the same (multiplied by a factor of 15) as that of $\partial u_1/\partial x_1$, while the spectrum of the full energy dissipation rate $\phi_{\epsilon_f}(k_1)$ is the sum of the spectra of the velocity gradients involved in Eq. (8), which are different from that of $\partial u_1/\partial x_1$. The departure of ϕ_{iso} from the other measures in Fig. 4 is therefore not surprising. This result indicates that the use of the instantaneous values of $\epsilon_{\rm iso}$ as a substitute of the instantaneous values of ϵ, as usually used in experimental studies, may cause significant errors, at least in the spectral domain. The satisfactory agreement at high wave numbers indicates that local isotropy is satisfied by various approximations to energy dissipation rate, even at a relatively low Reynolds number.

IV. CORRELATION BETWEEN ENERGY DISSIPATION RATE AND ENSTROPHY

Using the four-wire probe, only one component (ω_3) of the enstrophy can be measured. By assuming local isotropy, the instantaneous values of Ω can be obtained using

$$\Omega = 3\nu\omega_k^2 \ (k=1,2,\text{or } 3). \tag{12}$$

All three vorticity components in the full expression of Ω can be measured using the present eight-wire probe. The enstrophy can then be calculated as

$$\Omega = \nu(\omega_1^2+\omega_2^2+\omega_3^2). \tag{13}$$

The spatial correlations between ϵ and Ω can be quantified by means of conditional statistics, $\langle\beta|\alpha\rangle$, the expectations of β conditioned on particular values of α. This conditional expectation is defined as

$$\langle\beta|\alpha\rangle = \int_{-\infty}^{+\infty}\beta \mathrm{p}(\beta|\alpha)d\beta, \tag{14}$$

where $\mathrm{p}(\beta|\alpha)\equiv \mathrm{p}_{\alpha,\beta}/\mathrm{p}_\alpha$ is the pair distribution function (PDF) of β conditioned on α. These conditional expectations will be examined using various definitions of the energy dissipation rate. Figure 5 shows the conditional expectations $\langle\epsilon|\Omega\rangle/\langle\epsilon\rangle$ measured on the wake centerline. The values $\langle\epsilon_f|\Omega\rangle/\langle\epsilon_f\rangle$ increase linearly with ω_3^2 at an overall gradient of 0.87, reflecting a strong dependence of ϵ on Ω. The magnitude of $\langle\epsilon_{ap}|\omega_3^2\rangle/\langle\epsilon_{ap}\rangle$ from the four-wire measurement shows the similar trend, except that its gradient is changed from 0.87 for the eight-wire measurements to 0.75. This may suggest a slightly lower correlation between ϵ_{ap} and ω_3^2than that between ϵ_f and Ω. Compared with $\langle\epsilon_{ap}|\omega_3^2\rangle/\langle\epsilon_{ap}\rangle$ and $\langle\epsilon_f|\omega_3^2\rangle/\langle\epsilon_f\rangle$, the values of $\langle\epsilon_{iso}|\omega_3^2\rangle/\langle\epsilon_{iso}\rangle$ increase slowly with $\omega_3^2/(\omega_3^2)$, indicating a much weaker correlation between ϵ and ω_3^2 when using ϵ_{iso} to represent ϵ. This result suggests again that using ϵ_{iso} as a substitute of ϵ should be reexamined, especially for instantaneous values.

The spatial correlation between Ω and ϵ can also be quantified by means of the conditional expectation $\langle\Omega_r^{n+}|\epsilon_r^+\rangle$, where the superscript + denotes that the quantities are normalized by their mean values, i.e., $(\omega_3^2)_r^+=(\omega_3^2)_r/\langle(\omega_3^2)\rangle$ and

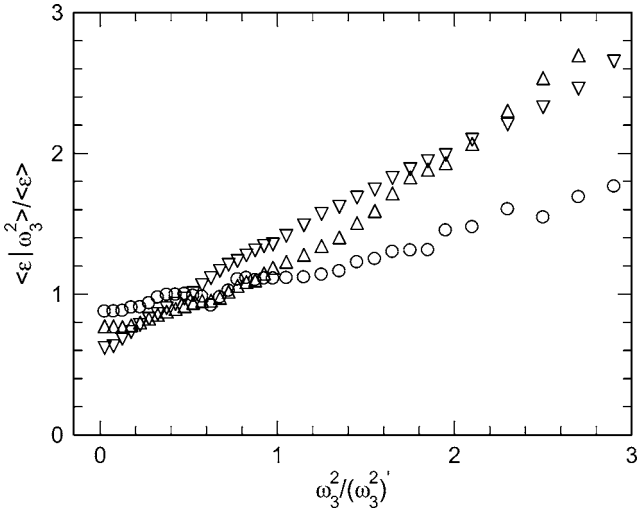

FIG. 5. Expectations of ϵ conditioned on particular values of ω_3^2: ∇, $\langle\epsilon_{ap}|\omega_3^2\rangle$ [Eq. (2)]; Δ, $\langle\epsilon_f|\omega_3^2\rangle$ [Eq. (8)]; and ○, $\langle\epsilon_{iso}|\omega_3^2\rangle$ [Eq. (1)].

$\epsilon_r^+=\epsilon_r/\langle\epsilon\rangle$; ϵ_r and Ω_r are the average values of ϵ and Ω obtained over a distance r in the streamwise direction. The conditional expectations $\langle(\omega_3^2)_r^{n+}|(\epsilon_{ap})_r^+\rangle$ for $n=1$ and 2 measured using the four-wire probe are shown in Fig. 6 to check the spatial correlation between the two quantities. The value of r is chosen such that it is located in the inertial range. It needs to be noted that an inertial range is not expected at such a low Reynolds number ($R_\lambda=45$). Arguably, a scaling range (SR) over which the third-order velocity structure function $\langle|\delta S_L^*|^3\rangle$ is approximately linear to r can be defined (Fig. 7), where $\delta S_L[\equiv u_1(x_1+r)-u_1(x_1)]$ is the longitudinal velocity structure function. The functions $y=c_1x$ and $y=c_2x^2$ are also included in Fig. 6, where c_1 and c_2 are constants determined by the curve fitting. It shows clearly that the first- and second-order moments of $(\omega_3^2)_r^+$ increase with

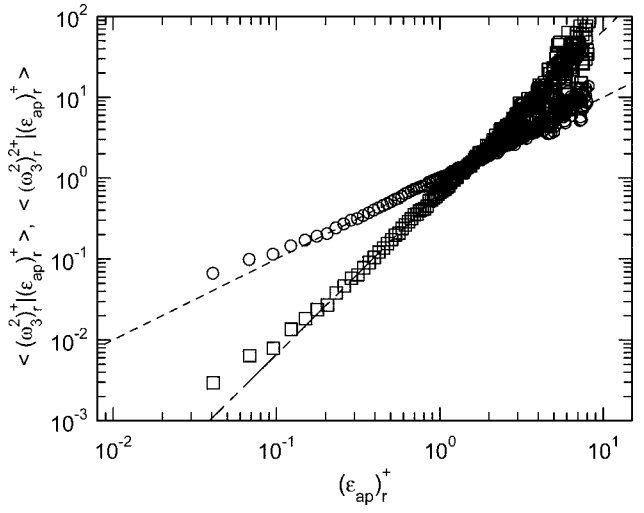

FIG. 6. Conditional expectations $\langle(\omega_3^2)_r^{n+}|(\epsilon_{ap})_r^+\rangle$ as a function of ϵ_{ap} using the four-wire probe: ○, $n=1$; □, $n=2$; - - -, $y=c_1x$; and — · —, $y=c_2x^2$.

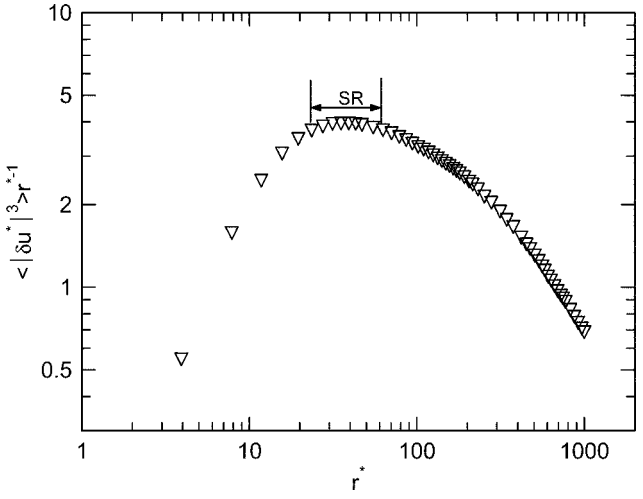

FIG. 7. Kolmogorov normalized third-order structure function multiplied by r^{*-1}.

ϵ_r^+. The values of $\langle(\omega_3^2)_r^+|(\epsilon_{ap})_r^+\rangle$ grow linearly with $(\epsilon_{ap})_r^+$ over the range of $\epsilon_r^+>0.1$. They also agree quite well with $y=c_2x^2$ in this range. These results imply a strong spatial correlation between the spanwise vorticity and the energy dissipation rate. The present results are consistent with the DNS study by Chen *et al.* [17], where the full energy dissipation rate and enstrophy Ω were used. When ϵ_{iso} is used (Fig. 8), even though the first- and second-order moments of $(\omega_3^2)_r^+$ increase with $(\epsilon_{iso})_r^+$, the gradients become much smaller than those shown in Fig. 6. The results seem to suggest that the use of the one-dimensional energy dissipation rate to substitute the full energy dissipation rate may lead to erroneous conclusions. To validate the present four-wire results and to clarify the different behaviors between ϵ_{iso} and ϵ_f, the expectations of $\langle(\omega_3^2)_r^n\rangle$ ($n=1$ and 2) conditioned on either ϵ_f or ϵ_{iso} obtained from the eight-wire probe are shown in Figs. 9 and 10, respectively. In Fig. 9, $\langle(\omega_3^2)_r^+|(\epsilon_f)_r^+\rangle$ and $\langle(\omega_3^2)_r^{2+}|(\epsilon_f)_r^+\rangle$ reveal almost the identical trends as those

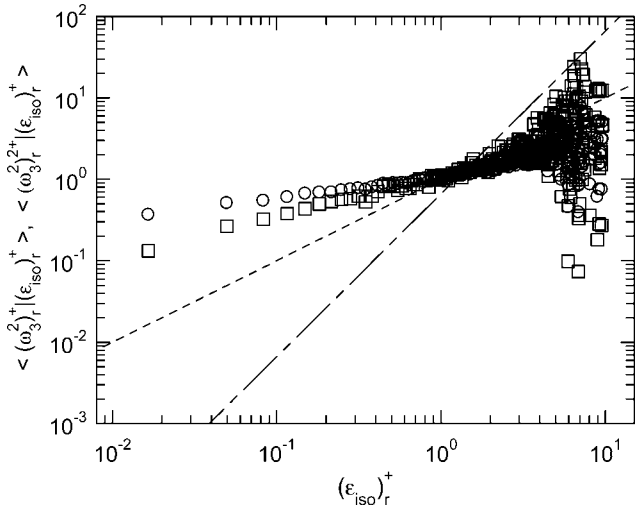

FIG. 8. Conditional expectations $\langle(\omega_3^2)_r^{n+}|(\epsilon_{iso})_r^+\rangle$ as a function of ϵ_{iso} using four-wire probe: ○, $n=1$; □, $n=2$; - - -, $y=c_1x$; and — · —, $y=c_2x^2$.

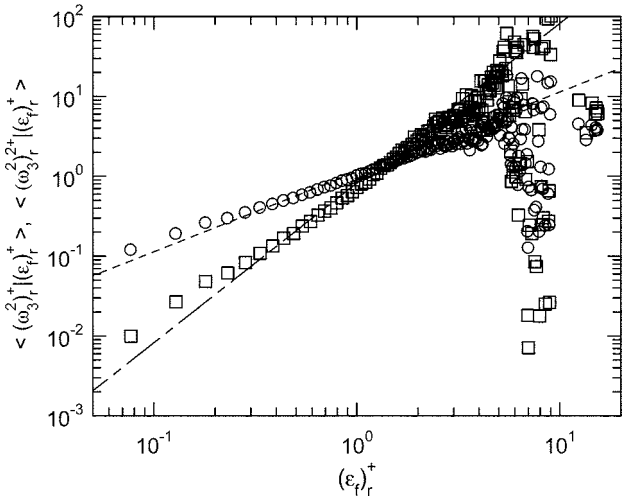

FIG. 9. Conditional expectations $\langle (\omega_3^2)_r^{n+} | (\epsilon_{ful})_r^+ \rangle$ as a function of $(\epsilon_f)_r^+$ using eight-wire probe: ○, $n=1$; □, $n=2$; - - -, $y=cx$; and — · —, $y=c_2x^2$.

shown in Fig. 6, and both of them agree well with functions $y=c_1x$ and $y=c_2x^2$, respectively, thus proving the strong correlation between the spanwise vorticity and the energy dissipation rate. The results also support the use of Eq. (2) as a proper substitute to the full energy dissipation rate. In Fig. 10, the expectations of $\langle (\omega_3^2)_r^n \rangle$ ($n=1$ and 2) conditioned on ϵ_{iso} show large discrepancies with those obtained using ϵ_f (Fig. 9). The discrepancy between Figs. 9 and 10 further implies that it is inappropriate to use ϵ_{iso} as a substitute of ϵ.

To further study the correlation between ϵ and Ω, the conditional expectations $\langle \Omega_r^{n+} | (\epsilon_f)_r^+ \rangle$ and the reverse conditional expectations $\langle (\epsilon_f)_r^{n+} | \Omega_r^+ \rangle$ for different orders ($n=1$, 2, 4, 6, and 8) are also examined. These results are shown in Figs. 11(a)–11(e). The data used in this figure for ϵ and Ω are measured using the eight-wire probe. It is found that while $\langle \Omega_r^{n+} | (\epsilon_f)_r^+ \rangle$ scales with $(\epsilon_f)_r^{\alpha n+}$ for large values of $(\epsilon_f)_r^+$, the

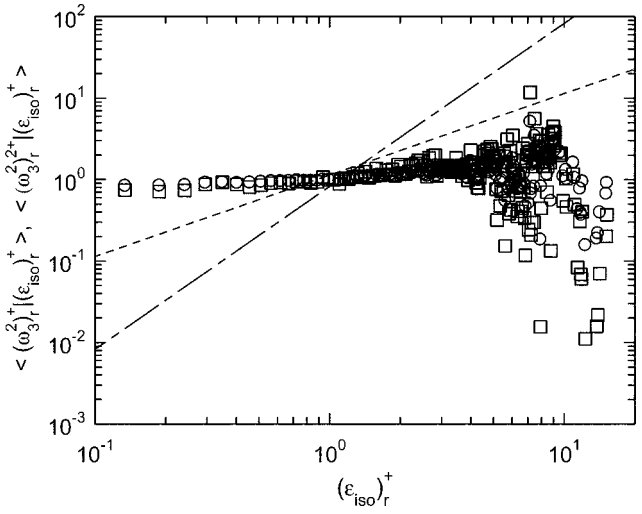

FIG. 10. Conditional expectations $\langle (\omega_3^2)_r^{n+} | (\epsilon_{iso})_r^+ \rangle$ as a function of $(\epsilon_{iso})_r^+$ using eight-wire probe: ○, $n=1$; □, $n=2$; - - -, $y=c_1x$; and — · —, $y=c_2x^2$.

reversed conditional expectations $\langle (\epsilon_f)_r^{n+} | \Omega_r^+ \rangle$ seem to scale with $\Omega_r^{\beta n+}$ for large Ω_r^+, with $\beta < \alpha \leq 1$. For example, when $n=1$ [Fig. 11(a)], the values of $\langle \Omega_r^+ | (\epsilon_f)_r^+ \rangle$ grow linearly with $(\epsilon_f)_r^+$ over the range of $(\epsilon_f)_r^+ > 0.06$ ($\alpha=1$ in this case), reflecting a strong correlation between enstrophy and energy dissipation rate. The same conclusion can be obtained for the distribution of $\langle (\epsilon_f)_r^+ | \Omega_r^+ \rangle$, which grows with Ω_r^+ by a power law of 0.953 ($\beta=0.953$ in this case) for $\Omega_r^+ > 0.6$. While for $n=6$ [Fig. 11(d)], the dependence of $\langle \Omega_r^{6+} | (\epsilon_f)_r^+ \rangle$ on $(\epsilon_f)_r^+$ over the range of $(\epsilon_f)_r^+ > 0.3$ shows an approximate power law of 5.7 (or $\alpha=0.951$); the power is 4.5 ($\beta=0.752$ in this case) for distribution of $\langle (\epsilon_f)_r^{6+} | \Omega_r^+ \rangle$ over the range of $\Omega_r^+ > 0.6$. The values of α and β for different powers n are listed in Table I. It can be seen that while both α and β decrease with the increase of n, the values of α are always larger than the corresponding values of β, with a much lower decreasing rate than that of β. The fact that α is larger than β with a lower decreasing rate may suggest that the spatial growth of ϵ_r^+ in a statistical sense is slower than that of Ω_r^+. It is worthy to note that the present results are consistent with the DNS study by Chen *et al.* [17], who also found that although strong domain correlation exists between ϵ and Ω, they are not correlated point by point.

V. SCALING OF LOCALLY AVERAGED ENSTROPHY AND ENERGY DISSIPATION RATES

Over the past years, extensive experimental and numerical investigations have highlighted the difference between the scaling exponents $\zeta_L(n)$ and $\zeta_T(n)$ of longitudinal and transverse velocity increments, respectively. In the present study, the longitudinal velocity structure function δS_L is defined as

$$\delta S_L = \delta u_1(r) = u_1(x_1 + r) - u_1(x_1). \tag{15}$$

Taylor's hypothesis is used to convert the temporal delay τ to a spatial increment r in the streamwise direction, with $r \equiv \tau U$, where U is the mean velocity in the streamwise direction. The transverse velocity structure function can then be defined as

$$\delta S_T = u_2(x_1 + r) - u_2(r). \tag{16}$$

In the present study, due to the limited value of R_λ studied, an apparent inertial range cannot be defined unambiguously (please refer to Fig. 7). To obtain the scaling exponents of the velocity structure functions, the extended self-similarity (ESS) method [23] is used. This method has been widely used for estimating the scaling exponents. The corresponding scaling exponents are known as the values relative to the third-order velocity increments. All the scaling exponents are estimated over the scaling range shown in Fig. 7. By plotting the nth-order velocity structure functions against the third-order moment of $|\delta S_L|$, i.e.,

$$\langle |\delta S_L|^n \rangle \sim \langle |\delta S_L|^3 \rangle^{\zeta_L(n)} \tag{17}$$

and

$$\langle |\delta S_T|^n \rangle \sim \langle |\delta S_L|^3 \rangle^{\zeta_T(n)}, \tag{18}$$

the longitudinal and transverse scaling exponents $\zeta_L(n)$ and $\zeta_T(n)$ can be estimated. The values of $\zeta_L(n)$ and $\zeta_T(n)$ for n

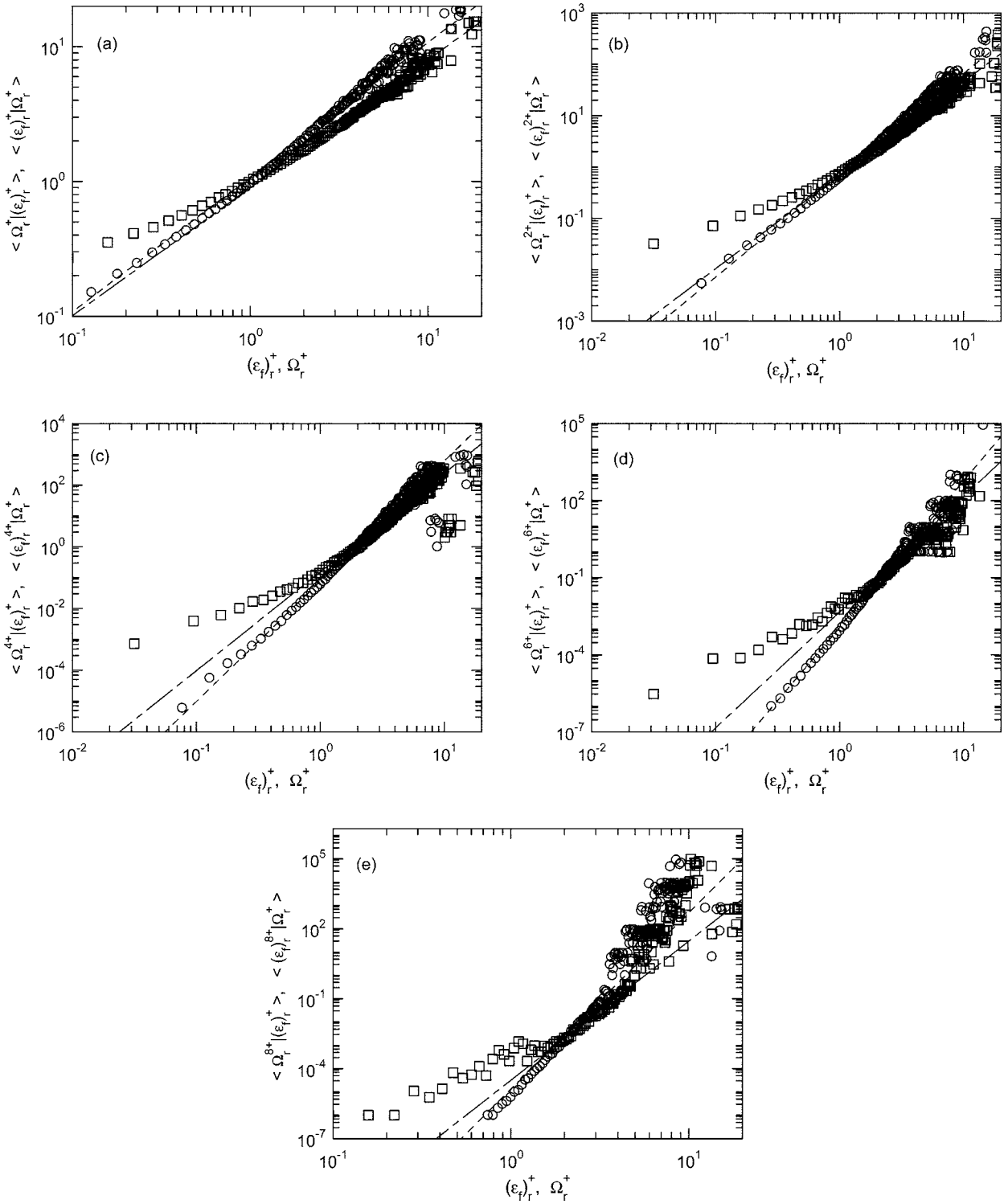

FIG. 11. Conditional expectations $\langle \Omega_r^{n+} | (\epsilon_f)_r^+ \rangle$ and $\langle (\epsilon_f)_r^{n+} | \Omega_r^+ \rangle$ as a function of ϵ_f^+ and Ω_r^+, respectively: ○, $\langle \Omega_r^{n+} | (\epsilon_f)_r^+ \rangle$; □, $\langle (\epsilon_f)_r^{n+} | \Omega_r^+ \rangle$; - - -, $y = c_1 x^{\alpha n}$; and — · —, $y = c_2 x^{\beta n}$; (a) $n=1$; $\alpha=1$, $\beta=0.953$; (b) $n=2$; $\alpha=0.993$, $\beta=0.917$; (c) $n=4$; $\alpha=0.975$, $\beta=0.813$; (d) $n=6$; $\alpha=0.951$, $\beta=0.752$; and (e) $n=8$; $\alpha=0.947$, $\beta=0.746$.

$=1-8$ are shown in Fig. 12. The predictions of the scaling exponents based on Kolmogorov [24] or K41, where the velocity structure functions are scaled as $n/3$, and the lognormal model of Kolmogorov [11] or K62 are also shown for comparison. For K62,

$$\zeta_L(n) = \frac{n}{3} - \frac{\mu}{18} n(n-3), \tag{19}$$

where μ is the intermittency parameter with a magnitude of $0.2 \sim 0.3$. The value of μ can be obtained using the 6th-order

TABLE I. The values of α and β for different orders of n.

n	1	2	4	6	8
α	1.00	0.993	0.975	0.951	0.947
β	0.953	0.917	0.813	0.752	0.746

velocity structure function, since $\langle(\delta S_L)^6\rangle \sim r^{2-\mu}$ [i.e., $\mu=2-\zeta_L(6)$] in the scaling range. The values of $\zeta_L(n)$ depart significantly from the prediction of K41 [24] (i.e., $n/3$) for $n>4$. This result may reflect the increasing effect of the intermittency for higher orders of the longitudinal velocity increments. The measured values of $\zeta_L(n)$ show satisfactory agreement with that predicted by K62 [11]. It can be seen that $\zeta_T(n)$ values are significantly smaller than $\zeta_L(n)$.

The inequality between $\zeta_L(n)$ and $\zeta_T(n)$ may be due to several factors: (1) the Reynolds number effect (e.g., [25–27]); (2) global anisotropy of the flow (e.g., [28–30]); (3) the initial and boundary conditions [31], and (4) the effects of intermittencies on the longitudinal and transverse velocity structure functions [32]. Analogous to the refined similarity hypothesis (RSH) [11], Chen *et al.* [32] proposed a modification which they called the refined similarity hypothesis for transverse velocity structure functions (RSHT). In RSH and RSHT, the scaling of the longitudinal and transverse velocity structure functions are

$$\zeta_\epsilon(n) = \frac{n}{3} + \tau_\epsilon(n/3) \tag{20}$$

and

$$\zeta_\Omega(n) = \frac{n}{3} + \tau_\Omega(n/3), \tag{21}$$

where $\tau_\epsilon(n/3)$ and $\tau_\Omega(n/3)$ are the scaling exponents of the locally averaged energy dissipation rate and the enstrophy,

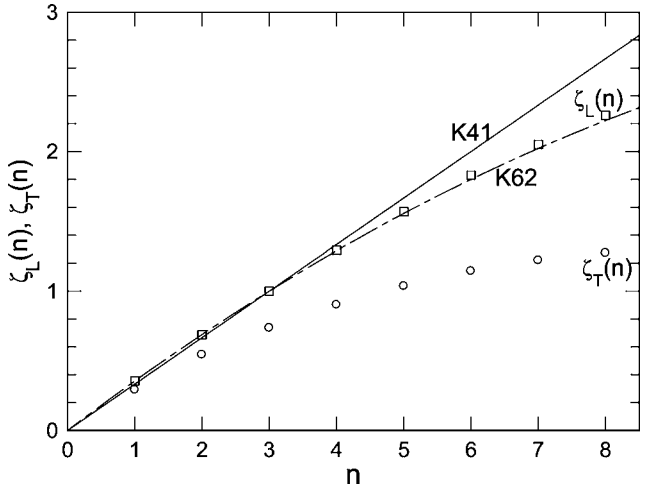

FIG. 12. Scaling exponents $\zeta_L(n)$ and $\zeta_T(n)$ as a function of n: □, $\zeta_L(n)$; ○, $\zeta_r(n)$; ——, K41 (Ref. [24]); and — · —K62 (Ref. [11].

respectively. They are inferred from the distributions of $\log\langle\epsilon_r^{n/3}\rangle$ and $\log\langle\Omega_r^{n/3}\rangle$ vs $\log r$ over the scaling range indicated in Fig. 7. The values of $\tau_\epsilon(n/3)$ and $\tau_\Omega(n/3)$ can be inferred based on various approximations to ϵ and Ω considered in the present study. These values are listed in Table II. The values of $\zeta_\epsilon(n)[\equiv(n/3)+\tau_\epsilon(n/3)]$ and $\zeta_\Omega(n)[\equiv(n/3)+\tau_\Omega(n/3)]$ as well as the measured $\zeta_L(n)$ and $\zeta_T(n)$ are also included in Table II for comparison. If RSH is valid, there should be favorable agreement between $\zeta_L(n)$ and $\zeta_\epsilon(n)$. The values shown in Table II indicate that $\zeta_{\epsilon_f}(n)$ and $\zeta_{\epsilon_{ap}}(n)$ agree well with $\zeta_L(n)$ for all orders. Both of them are smaller than $\zeta_{\epsilon_{iso}}(n)$ for $n\leq 2$ and slightly larger than $\zeta_{\epsilon_{iso}}(n)$ $n\geq 3$. This result indicates that for ε_{ap} is a proper substitute to ϵ_f, while ϵ_{iso} is more intermittent than either ϵ_f or ϵ_{ap}. The later result is consistent with previous investigations reported by

TABLE II. Scaling exponents of the velocity structure functions, energy dissipation rates, and enstrophy. The values in the brackets represent the corresponding standard deviations.

n	$\zeta_L(n)$	$\zeta_T(n)$	$\tau_{\epsilon_f}(n)$	$\zeta_{\epsilon_f}(n)$	$\tau_{\epsilon_{ap}}(n)$	$\zeta_{\epsilon_{ap}}(n)$	$\tau_{\epsilon_{iso}}(n)$	$\zeta_{\epsilon_{iso}}(n)$	$\tau_\Omega(n)$	$\zeta_\Omega(n)$	$\tau_{\Omega_3^2}(n)$	$\zeta_{\Omega_3^2}(n)$
1	0.356	0.292	0.01 (±0.001)	0.343	0.0188 (±0.001)	0.352	0.0348 (±0.001)	0.368	0.0222 (±0.001)	0.356	0.0531 (±0.001)	0.386
2	0.688	0.545	0.009 (±0.001)	0.676	0.0182 (±0.001)	0.685	0.0324 (±0.001)	0.699	0.0219 (±0.001)	0.689	0.044 (±0.001)	0.711
3	1	0.736	−0.01 (±0.0013)	0.99	−0.0082 (±0.001)	0.992	−0.0088 (±0.001)	0.99	−0.00613 (±0.001)	0.994	−0.01 (±0.001)	0.99
4	1.293	0.902	−0.0452 (±0.0013)	1.288	−0.0591 (±0.001)	1.274	−0.0838 (±0.001)	1.25	−0.0594 (±0.001)	1.274	−0.103 (±0.001)	1.23
5	1.568	1.037	−0.097 (±0.001)	1.57	−0.132 (±0.001)	1.535	−0.1879 (±0.001)	1.479	−0.1353 (±0.0011)	1.531	−0.227 (±0.0011)	1.44
6	1.83	1.144	−0.164 (±0.004)	1.836	−0.228 (±0.001)	1.772	−0.3173 (±0.0013)	1.683	−0.2319 (±0.0015)	1.768	−0.378 (±0.001)	1.622
7	2.05	1.222	−0.2461 (±0.0015)	2.09	−0.343 (±0.001)	1.99	−0.4685 (±0.0014)	1.864	−0.3468 (±0.002)	1.987	−0.55 (±0.001)	1.783
8	2.26	1.273	−0.3423 (±0.0015)	2.32	−0.475 (±0.0013)	2.192	−0.6387 (±0.0015)	2.028	−0.478 (±0.0028)	2.189	−0.739 (±0.0012)	1.928

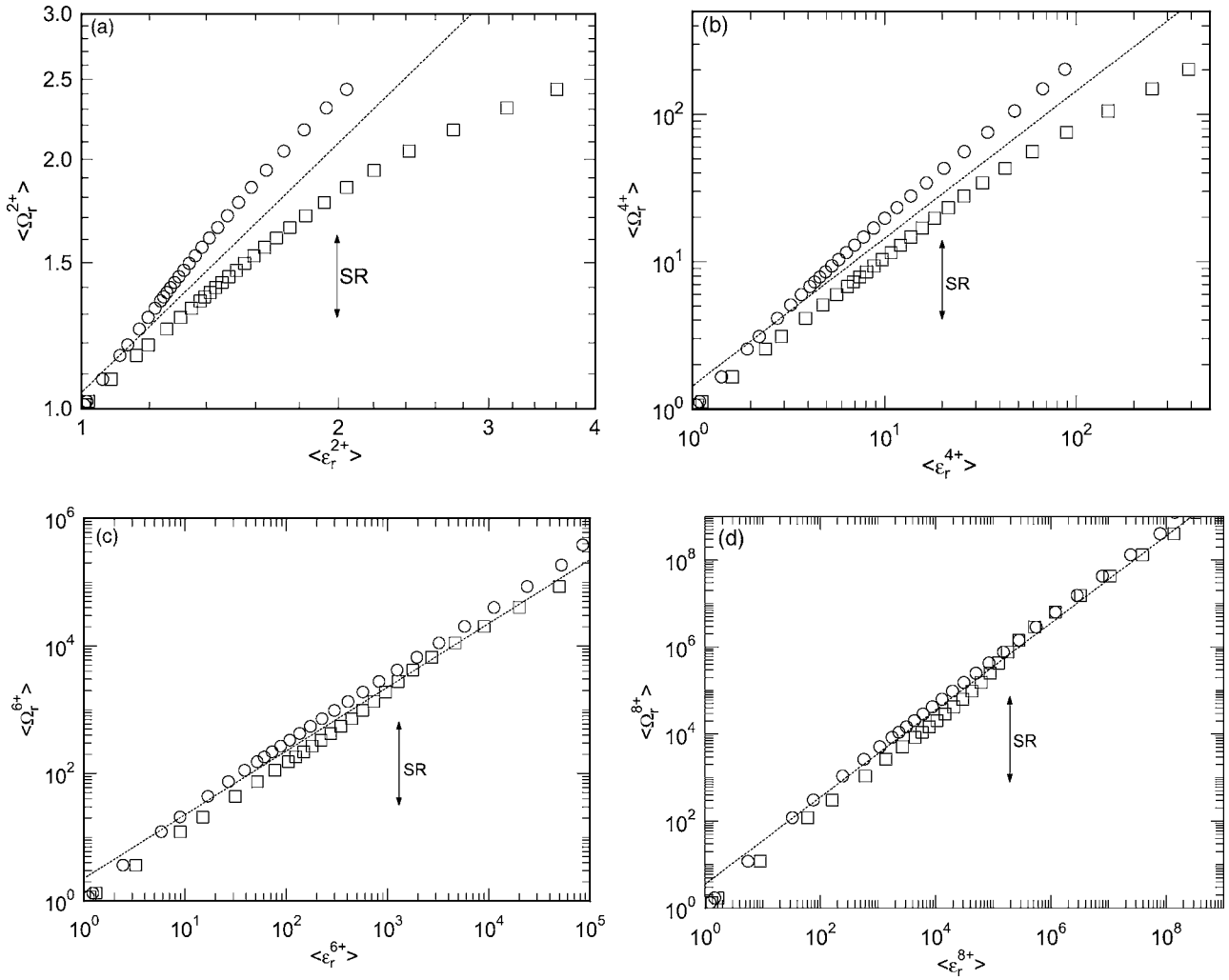

FIG. 13. $\langle \Omega_r^n \rangle$ as a function of $\langle \epsilon_r^n \rangle$. Here r is an implicit variable. ○, obtained using ϵ_f [Eq. (8)]; □, obtained using ϵ_{iso} [Eq. (1)]; and ·····, $y=x$. Arrowed vertical line indicates points within inertial range. (a) $n=2$; (b) $n=4$; (c) $n=6$; (d) $n=8$.

Sreenivasan and Antonia [16], Chen *et al.* [32], and Wang *et al.* [12]. If RSHT is valid, the difference between $\zeta_L(n)$ and $\zeta_T(n)$ should be compensated by the difference between $\zeta_\epsilon(n)$ and $\zeta_\Omega(n)$ or $\tau_\epsilon(n/3)$ and $\tau_\Omega(n/3)$, respectively. However, the results shown in Table II indicate that the magnitude $\zeta_L(n)-\zeta_T(n)$ is much larger than that of $\zeta_\epsilon(n)-\zeta_\Omega(n)$, regardless of the methods used to obtain ϵ and Ω. Therefore, RSHT is only partially valid for the temporal transverse velocity increments obtained by using Taylor's hypothesis. This result is in contrary to that reported by Bi and Wei [33], where the transverse velocity structure functions were obtained using both the temporal and spatial methods; the energy dissipation rate ϵ and enstrophy Ω were approximated by ϵ_{iso} and $3\nu\omega_2^2$, respectively. Comparing the values for $\tau_\Omega(n/3)$ and $\tau_{\omega_3^2}(n/3)$, we can see that the former is consistently smaller than the latter. It is worthy to note that the present magnitude of $\tau_\Omega(n/3)$ is comparable with those reported by Antonia *et al.* [6] in a grid turbulence, while the values of $\tau_{\omega_3^2}(n/3)$ are also comparable to those reported by Zhou *et al.* [34] in a cylinder wake. The results shown in Table II indicate that the full enstrophy [Eq. (13)] is less intermittent than its individual vorticity component [Eq. (12)]. The values in Table II also indicate that the enstrophy field is more intermittent than the energy dissipation rate. To get a better understanding on the intermittency phenomena and to study the scaling features of enstrophy and energy dissipation, it is necessary to examine the scaling relation between the higher-order moment of enstrophy and those of energy dissipation rate. Wang *et al.* [12], in their DNS studies, pointed out that for the energy dissipation rate, the one-dimensional surrogate field is in general more intermittent than the full field. Both the isotropic [Eq. (1)] and the full energy dissipation rate [Eq. (8)] are used to examine the relative scaling with the enstrophy. In Figs. 13(a)–13(d), the quantities $\langle \Omega_r^{n+} \rangle$ are plotted against $\langle \varepsilon_r^{n+} \rangle$ for $n=2$, 4, 6, and 8. The relative power laws can be identified in the scaling range (a region indicated by the double-arrowed vertical line) and quantified by the scaling exponent k, which is calculated from $\langle \Omega_r^{n+} \rangle \sim \langle \epsilon_r^{n+} \rangle^k$. For convenience, the values of k for different orders n are listed in Table III. It can be seen that the values of $k(\epsilon_f)$ are always greater than 1 for $n=2$, 4, 6, and 8. This result shows that the locally averaged full enstrophy are larger than those of locally averaged full dissipation

TABLE III. Scaling exponents k in $\langle \Omega_r^n \rangle \sim \langle \epsilon_r^n \rangle^k$ obtained from the full [Eq. (8)] and one-dimensional isotropic [Eq. (1)] energy dissipation rate for $n=2,4,6,8$.

N	2	4	6	8
$k(\epsilon_f)$	1.39	1.32	1.07	1.05
$k(\epsilon_{iso})$	0.84	0.92	1.03	1.04

rate, indicating a stronger intermittency of the former than the latter, which is consistent with Chen *et al.* [17]. The present values of $k(\epsilon_f)$ are qualitatively close to those of the DNS study by Chen *et al.* [17], where $k=1.56$ and 1.47 for $n=2$ and 4, respectively, were obtained. It can also be seen that $k(\epsilon_f)$ decreases with the increase of n. The values of $k(\epsilon_{iso})$ obtained using $\langle \Omega_r^n \rangle \sim \langle (\epsilon_{iso})_r^n \rangle^k$ increases with n, a reverse trend to that of $k(\epsilon_f)$. In addition, the fact that the values of $k(\epsilon_{iso})$ obtained using $\langle \Omega_r^n \rangle \sim \langle (\epsilon_{iso})_r^n \rangle^k$ are much smaller than that of $k(\epsilon_f)$, especially for $n=1$ and 2, suggests that the intermittency of the dissipation rate based on isotropic relations is stronger than that of the full enstrophy, which is consistent with the results shown in Table II. The result also indicates that for the energy dissipation rate, the one-dimensional surrogate field is more intermittent than the full dissipation field, which is consistent with that reported by Wang *et al.* [12]. The differences in intermittency between ϵ_{iso} and ϵ_f may be due to the fact that the full energy dissipation rate involves all nine velocity derivatives while ϵ_{iso} involves only one (i.e., $\partial u_1/\partial x_1$). The full dissipation rate can be considered roughly as an average of nine intermittent structures, each of which is either as large as ϵ_{iso} or slightly larger than ϵ_{iso}. The averaging tends to reduce the degree of intermittency of individual structures [12].

VI. CONCLUSION

Different approximations to energy dissipation rate and enstrophy have been made using a four-wire probe and an eight-wire probe in the far field of a cylinder wake at Re $=2060$. There exists satisfactory agreement among the mean energy dissipation rates, regardless of the approximations used. However, spectral analysis shows that there is large departure of the spectrum of ϵ_{iso} from that of either ϵ_{ap} or ϵ_f at low wave numbers, indicating that the use of the instantaneous values of ϵ_{iso} as a substitute of the instantaneous values of ϵ, as usually used in experimental studies, may cause significant errors, at least in the spectral domain. The spatial correlation between ϵ (represented either by ϵ_{iso}, ϵ_{ap}, or ϵ_f) and Ω [represented either by Eq. (12) or Eq. (13)] has been qualified using conditional analysis. Compared with ϵ_{ap} and ϵ_f, there is a much weaker correlation between ϵ and Ω when ϵ_{iso} is used to represent ϵ. When ϵ_{ap} or ϵ_f is used, the conditional expectations $\langle \Omega_r^{n+} | (\epsilon_f)_r^+ \rangle$ ($n=1$ and 2) agree well with $y=cx^n$ in the scaling range, further confirming the strong correlation between energy dissipation rate and enstrophy. This result is consistent with that reported previously by Chen *et al.* [17] using DNS. The inertial range scaling exponents of the energy dissipation rate and enstrophy suggest that the energy dissipation rate based on isotropic relation is more intermittent than that of the true values, supporting the previous study by Wang *et al.* [12], while the isotropic enstrophy is more intermittent than the full enstrophy. It is also found that the full energy dissipation rate is less intermittent than the full enstrophy. The present study suggests that using ϵ_{iso} as a substitute of the true values for ϵ should be re-examined, especially for the instantaneous values.

[1] J. Cleve, M. Greiner, B. R. Pearson, and K. R. Sreenivasan, Phys. Rev. E **69**, 066316 (2004).
[2] C. Meneveau, K. R. Sreenivasan, P. Kailasnath, and M. Fan, Phys. Rev. A **41**, 894 (1990).
[3] G. Stolovitzky, P. Kailasnath, and K. R. Sreenivasan, J. Fluid Mech. **297**, 275 (1995).
[4] A. Tsinober, E. Kit, and T. Dracos, J. Fluid Mech. **242**, 169 (1992).
[5] B. Maralis, P. Nguyen, and J. M. Wallace, Exp. Fluids **15**, 209 (1993).
[6] R. A. Antonia, T. Zhou, and Y. Zhu, J. Fluid Mech. **374**, 29 (1998).
[7] Y. Zhu and R. A. Antonia, Exp. Fluids **27**, 21 (1999).
[8] G. P. Romano and R. A. Antonia, J. Fluid Mech. **436**, 231 (2001).
[9] C. Meneveau and K. R. Sreenivasan, Phys. Rev. Lett. **59**, 1424 (1987).
[10] G. Stolovitzky, P. Kailasnath, and K. R. Sreenivasan, Phys. Rev. Lett. **79**, 1178 (1992).
[11] N. Kolmogorov, J. Fluid Mech. **13**, 82 (1962).
[12] L.-P. Wang, S. Chen, J. Brasseur, and J. Wyngaard, J. Fluid Mech. **309**, 113 (1996).
[13] I. Hosokawa, J. Phys. Soc. Jpn. **64**, 3141 (1995).
[14] S. T. Thoroddsen, Phys. Fluids **7**, 691 (1995).
[15] I. Hosokawa, S. Oide, and K. Yamamoto, Phys. Rev. Lett. **77**, 4548 (1996).
[16] K. R. Sreenivasan and R. A. Antonia, Annu. Rev. Fluid Mech. **29**, 435 (1997).
[17] S. Y. Chen, K. R. Sreenivasan, and M. Nelkin, Phys. Rev. Lett. **79**, 1253 (1997).
[18] R. A. Antonia, Y. Zhu, and J. Kim, Exp. Fluids **15**, 65 (1993).
[19] T. Zhou and R. A. Antonia, Phys. Fluids **12**, 335 (2000).
[20] R. A. Antonia, Y. Zhu, and H. S. Shafi, J. Fluid Mech. **323**, 173 (1996).
[21] Y. Zhu and R. A. Antonia, Meas. Sci. Technol. **7**, 1492 (1996).
[22] L. W. B. Browne, R. A. Antonia, and D. A. Shah, J. Fluid Mech. **179**, 307 (1987).
[23] R. Benzi, S. Ciliberto, R. Tripiccione, C. Baudet, F. Massaioli, and S. Succi, Phys. Rev. E **48**, R29 (1993).
[24] N. Kolmogorov, Dokl. Akad. Nauk SSSR **30**, 301 (1941).
[25] B. Dhruva, Y. Tsuji, and K. R. Sreenivasan, Phys. Rev. E **56**, R4928 (1997).

[26] M. Nelkin, Am. J. Phys. **68**, 310 (2000).
[27] T. Zhou and R. A. Antonia, J. Fluid Mech. **406**, 81 (2000).
[28] V. L'vov and I. Procaccia, Phys. Fluids **8**, 2565 (1996).
[29] I. Arad, V. L'vov, and I. Procaccia, Phys. Rev. E **59**, 6753 (1999).
[30] G. P. Romano, R. A. Antonia, and T. Zhou, Exp. Fluids **27**, 368 (1999).
[31] R. A. Antonia and B. R. Pearson, Phys. Rev. E **62**, 8086 (2000).
[32] S. Y. Chen, K. R. Sreenivasan, M. Nelkin, and N. Cao, Phys. Rev. Lett. **79**, 2253 (1997).
[33] W. Bi and Q. Wei, J. Turbul. **4**, paper 28 (2003).
[34] T. Zhou, Z. Hao, L. P. Chua, and S. C. M. Yu, Phys. Rev. E **71**, 066307 (2005).